PHYSICAL SCIENCES

Capturing the radical ion-pair intermediate in DNA guanine oxidation

Jialong Jie,[1,3] Kunhui Liu,[2] Lidan Wu,[1] Hongmei Zhao,[1] Di Song,[1] Hongmei Su[1,2,3]*

Although the radical ion pair has been frequently invoked as a key intermediate in DNA oxidative damage reactions and photoinduced electron transfer processes, the unambiguous detection and characterization of this species remain formidable and unresolved due to its extremely unstable nature and low concentration. We use the strategy that, at cryogenic temperatures, the transient species could be sufficiently stabilized to be detectable spectroscopically. By coupling the two techniques (the cryogenic stabilization and the time-resolved laser flash photolysis spectroscopy) together, we are able to capture the ion-pair transient $G^{+\bullet}\cdots Cl^-$ in the chlorine radical–initiated DNA guanine (G) oxidation reaction, and provide direct evidence to ascertain the intricate type of addition/charge separation mechanism underlying guanine oxidation. The unique spectral signature of the radical ion-pair $G^{+\bullet}\cdots Cl^-$ is identified, revealing a markedly intense absorption feature peaking at 570 nm that is distinctive from $G^{+\bullet}$ alone. Moreover, the ion-pair spectrum is found to be highly sensitive to the protonation equilibria within guanine-cytosine base pair (G:C), which splits into two resolved bands at 480 and 610 nm as the acidic proton transfers along the central hydrogen bond from $G^{+\bullet}$ to C. We thus use this exquisite sensitivity to track the intrabase-pair proton transfer dynamics in the double-stranded DNA oligonucleotides, which is of critical importance for the description of the proton-coupled charge transfer mechanisms in DNA.

INTRODUCTION

With the lowest oxidation potential among all the nucleobases, guanine (G) is extremely redox-active and plays central roles in the processes of DNA oxidative damage (*1*, *2*) and DNA charge transfer (*3*–*5*). Upon the interaction of photoexcitation (*6*–*8*) or under the attack of potent radical oxidants (*1*, *2*, *9*–*13*), G is subject to a facile loss of an electron and forms a cation radical $G^{+\bullet}$ (hole) in the DNA strand, initiating the hole transfer that makes DNA a charge transfer wire (*4*, *14*) or leading to a cascade of DNA oxidative damage events (*15*). As is well known, $G^{+\bullet}$ may deprotonate or undergo nucleophilic addition reactions of water addition, leading to a variety of guanine lesion products (for example, 8-oxoG, FAPY-G, imidazolone, and oxazolone) (*2*, *16*) associated with the occurrence of degenerative diseases, cancer, and aging (*15*). Knowing the mechanisms and dynamics of guanine oxidation is critically important to understand DNA oxidative damage in the biological cellular process (*2*, *15*) as well as to the development of DNA-based electrochemical devices (*4*, *14*).

The formation of the oxidized radical product $G^{+\bullet}$ not only is a direct one-electron oxidation process but also frequently follows intricate mechanisms involving ion-pair intermediates, which are yet to be ascertained. In the photoinduced charge injection or electron transfer process in DNA, it is generally assumed that photoexcitation induces a charge separation between the intercalated photosensitizer and an adjacent guanine base, leading to a contact radical ion pair as the crucial intermediate (*17*–*21*). The ion pair is short-lived as a consequence of ultrafast charge recombination, a process that is strongly distance-dependent (*19*–*21*). In another aspect, when an oxidizing radical reacts with DNA guanine in aqueous media, the ion-pair mechanism may be invoked largely. For the hydroxyl radical $OH^\bullet$ oxidizing guanine, although never detected, a metastable ion-pair intermediate $G^{+\bullet}\cdots OH^-$ with a different structure and character from $G^{+\bullet}$ alone was predicted theoretically by density functional theory (DFT) calculations (*22*). After the initial addition of $OH^\bullet$ at C4=C5 double bond of guanine (*1*, *22*, *23*), charge separation between G and $OH^\bullet$ would lead to the formation of a metastable intermediate, the ion-pair $G^{+\bullet}\cdots OH^-$, which exists as local energy minimum in the potential energy surface and may play key roles in leading to final oxidation products (*1*, *22*, *23*). The possible formation of the ion pair could be ascribed to the highly oxidizing capability of the $OH^\bullet$ radical (*22*) and the ionizing nature of water (*24*). Virtually, ion pairing is one of the fundamental phenomena in chemistry and biology (*25*, *26*), and thus, it is of particular interest for chemists to identify and study this species.

Despite their pivotal roles, the unambiguous detection and characterization of this metastable radical ion-pair species remains formidable and unresolved due to the extremely low stability and concentration. Molecular dynamics simulations estimated the lifetime to be ~3 ps for the ion-pair species possibly involved when $OH^\bullet$ attacks the exocyclic NH_2 group of guanine (*27*). Even at ultrashort time scales, the intermediate has almost no accumulation of detectable concentration because of its instantaneous conversion into final products. Here, we use the strategy that, at low temperatures, the transient species could be sufficiently stabilized to be detectable spectroscopically. This fact has been extensively used in studying DNA radiation chemistry by electron spin resonance (ESR) spectroscopy (*11*, *12*) and infrared spectroscopy (*28*). Moreover, we couple the two techniques (the cryogenic stabilization and the time-resolved laser flash photolysis spectroscopy) together, which permits both the capture of the ion-pair transient and the direct observation of its formation and decay dynamics in real time.

The time-resolved spectroscopy detection at low temperature is nontrivial because it requires the use of conditions that maintain the transparent and homogeneous solution and that permit the transmission of the pump and probe light. The antifreeze agent LiCl is thus required to be dissolved with DNA samples, making an aqueous glassy solution for low-temperature laser flash photolysis experiments. Under this circumstance, radicals such as $OH^\bullet$ are inevitably consumed by reacting with the large excess of antifreeze agent

[1]Beijing National Laboratory for Molecular Sciences, Institute of Chemistry, Chinese Academy of Sciences, Beijing 100190, China. [2]College of Chemistry, Beijing Normal University, Beijing 100875, China. [3]University of Chinese Academy of Sciences, Beijing 100049, China.
*Corresponding author. Email: hongmei@iccas.ac.cn

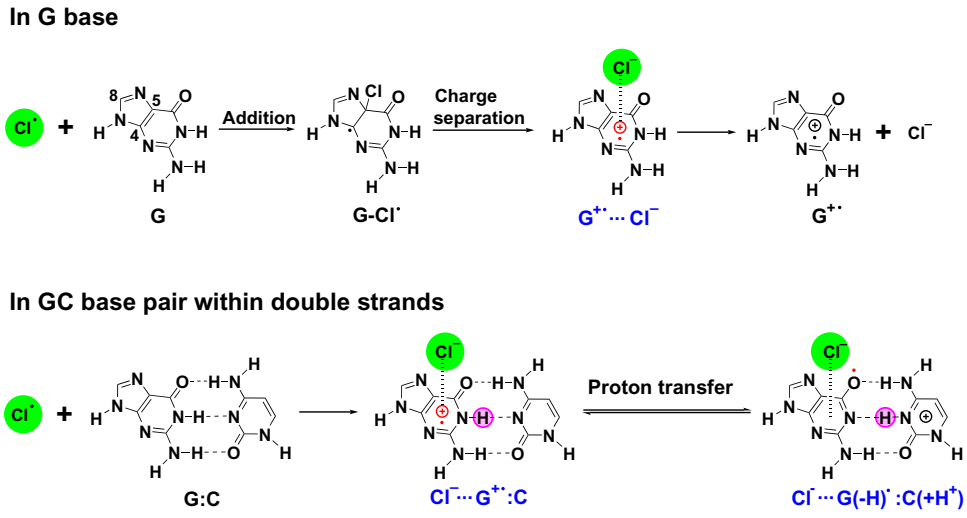

Fig. 1. The ion-pair species formed in the oxidation process of guanine in the G base and in the GC base pair within dsDNA separately.

LiCl, instead of undergoing reaction with DNA guanine. Alternatively, we use the photolysis of peroxodisulfate to produce $SO_4^{-\bullet}$, which reacts with LiCl and converts into chlorine radicals instantaneously. The chlorine radicals then react with guanine, initiating DNA guanine oxidation. This is also the normally adopted radical generation method in low-temperature ESR studies (*11*, *12*).

Specifically, the oxidation reactions of guanine in free deoxynucleoside and double-stranded oligonucleotides (dsDNA) by chlorine radicals (Fig. 1) are examined, from which the radical ion-pair transient $G^{+\bullet}\cdots Cl^-$ is directly observed in the low-temperature transient absorption spectra, showing a unique spectral signature with large absorption magnitude in the visible wavelength (570 nm) that is distinctive from $G^{+\bullet}$ alone. This intense visible absorption band is identified to be specific to the ion-pair $G^{+\bullet}\cdots Cl^-$ and well rationalized by time-dependent DFT (TD-DFT) calculations. It is further discovered that the ion-pair spectrum is highly sensitive to the protonation equilibria and base-pairing interactions in dsDNA, splitting into two resolved bands peaking at 480 and 610 nm as the acidic proton transfers along the central hydrogen bond from $G^{+\bullet}$ to C within the base pair (Fig. 1). We thus use this exquisite sensitivity of the ion-pair spectra to track the dynamics of the proton motion within the GC base pair, the so-called intrabase-pair proton transfer in duplex DNA, which is of critical importance for establishing the proton-coupled charge transfer mechanisms in DNA.

RESULTS AND DISCUSSION

Capture of the radical ion-pair $G^{+\bullet}\cdots Cl^-$ in the oxidation reaction of guanine base monomer

To prepare chlorine radicals, we adopt the conventional method of $SO_4^{-\bullet}$ oxidizing Cl^- (Eqs. 1 to 3), where the sulfate radicals $SO_4^{-\bullet}$ generated from the 355-nm photodissociation of peroxodisulfate anions ($S_2O_8^{2-}$) (*13*, *29*) react instantaneously with the high concentration Cl^- (7.0 M LiCl present as antifreeze agent) to yield $Cl^\bullet$, and $Cl^\bullet$, in turn, complexes with Cl^- to generate the chlorine radical ion $Cl_2^{-\bullet}$ (*11*, *12*, *30*). In this consecutive radical generation process, in principle, almost all of the former two radicals $SO_4^{-\bullet}$ and $Cl^\bullet$ are subject to conversion into $Cl_2^{-\bullet}$ within the laser pulse duration due to the fast reaction rate constants of Eqs. 2 and 3 (10^8 to 10^9 M^{-1} s^{-1}) (*30*, *31*) and the large concentration of Cl^- (7.0 M). It is seen in Fig. 2 (A and B) that the transient absorption band of $Cl_2^{-\bullet}$ (λ_{max} = 340 nm) (*30*, *32*) reaches its maximum intensity within 20 ns following the laser excitation

$$S_2O_8^{2-} \xrightarrow{h\nu} 2SO_4^{-\bullet} \quad (1)$$

$$SO_4^{-\bullet} + Cl^- \rightarrow SO_4^{2-} + Cl^\bullet \quad (2)$$

$$Cl^\bullet + Cl^- \rightarrow Cl_2^{-\bullet} \quad (3)$$

The sucessive reaction of chlorine radical oxidizing deoxyguanosine (dG) was first monitored at room temperature (298 K; Fig. 2C). Because of the efficient reaction with dG, the decay of the $Cl_2^{-\bullet}$ band at 340 nm is accelerated, which is accompanied by the buildup of a transient feature with broad absorption bands at 310, 390, and 510 nm within ~5 μs. This is the characteristic absorption pattern for $G^{+\bullet}$ and its deprotonated neutral form $G(-H)^\bullet$ (*13*, *29*, *33*, *34*). The product $G^{+\bullet}$ should result from the one-electron oxidation of G by $Cl_2^{-\bullet}$ (Eq. 4), which is followed by rapid deprotonation (loss of the imino proton) to $G(-H)^\bullet$ (1.8×10^7 s^{-1}) (*33*), as is well known.

$$Cl_2^{-\bullet} + G \rightarrow 2Cl^- + G^{+\bullet} \quad (4)$$

$$SO_4^{-\bullet} + G \rightarrow SO_4^{2-} + G^{+\bullet} \quad (5)$$

$$Cl^\bullet + G \rightarrow Cl^- + G^{+\bullet} \quad (6)$$

Strikingly, a distinct absorption band pointing to a new species emerges in the transient spectra detected at low temperature (230 K; Fig. 2D). In addition to the 340-nm band of $Cl_2^{-\bullet}$ and its temporal evolution into $G^{+\bullet}/G(-H)^\bullet$ (310, 390, and 510 nm), a strong absorption band at ~570 nm is observed prominently. There are some observations and facts that are pertinent to the assignment of this new transient.

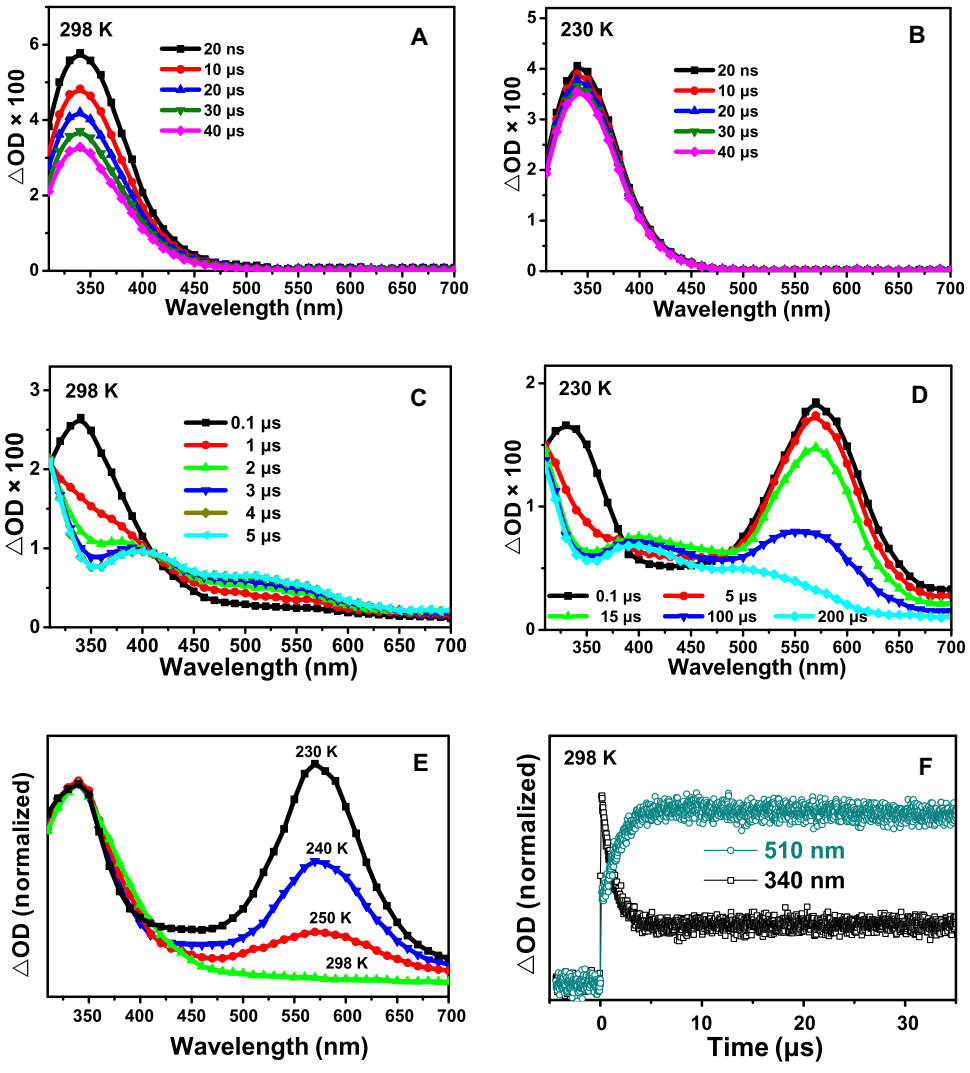

Fig. 2. Oxidation of G monomer. Transient absorption spectra obtained after 355-nm laser flash photolysis of $Na_2S_2O_8$ + LiCl at 298 K (**A**) and at 230 K (**B**). OD, optical density. Transient absorption spectra obtained after 355-nm laser flash photolysis of $Na_2S_2O_8$ + LiCl + dG at 298 K (**C**) and at 230 K (**D**). (**E**) Time slice (0.1 μs) of the transient absorption spectra obtained after 355-nm laser flash photolysis of $Na_2S_2O_8$ + LiCl + dG at different temperatures. (**F**) Normalized absorption changes at 340 and 510 nm after laser flash photolysis of $Na_2S_2O_8$ + LiCl + dG at 298 K. The concentration of $Na_2S_2O_8$, LiCl, and dG used in above experiments is 150 mM, 7.0 M, and 4 mM, respectively.

(i) The possibility of this species produced during the radical generation process can be ruled out because no 570-nm transient is seen in the 230 K blank experiment in the absence of dG (Fig. 2B). (ii) The deoxyribose group in dG is inert against radical oxidation, and no reaction signals were detected with the deoxyribose sample in the control experiment. (iii) This 570-nm transient is not ascribed to $G^{+\bullet}$ or $G(-H)^{\bullet}$ that is featured with only weak and flat absorptions above 500 nm. (iv) The possible contribution of sequential oxidation events of guanine can be excluded because the 570-nm transient completes its formation within ~0.1 μs, which is before the slow $Cl_2^{-\bullet}$ decay and $G^{+\bullet}/G(-H)^{\bullet}$ formation. (v) The 570-nm band intensity strongly depends on the temperature and increases markedly with the decreasing temperature (Fig. 2E), indicating that it is most likely ascribed to a new transient species with low stability that can only be captured at low temperatures. Here, while allowing the 570-nm transient to be stabilized and captured, the temperatures down to 230 K were tested to maintain the liquid state of solution with sufficient diffusion such that bimolecular reaction between the oxidizing radical and G could occur. When temperatures were lowered further below 200 K, the signal magnitude of transient products decreased because of the less bimolecular reaction events occurring.

For the 570-nm new transient captured at low temperatures, as shown in Fig. 2D, its formation time is within 0.1 μs and obviously not correlated with the decay of the 340-nm $Cl_2^{-\bullet}$ band (~15 μs). The decay of $Cl_2^{-\bullet}$ corresponds to the one-electron oxidation of G + $Cl_2^{-\bullet}$ (Eq. 4), with the concomitant formation of the feature product $G^{+\bullet}/G(-H)^{\bullet}$ at 390 nm and a slower rate (~15 μs) than that at room temperature. According to its rise kinetics (~0.1 μs), the new transient at 570 nm is not from the one-electron oxidation of G by $Cl_2^{-\bullet}$ but rather originates from a parallel competing reaction, most likely the direct oxidation of G by either of two other highly reactive radicals $SO_4^{-\bullet}$ and $Cl^{\bullet}$ (Eqs. 5 and 6) that are before the $Cl_2^{-\bullet}$ radical generation. Although almost all $SO_4^{-\bullet}$ and $Cl^{\bullet}$ radicals are presumably converted into $Cl_2^{-\bullet}$ within ~20 ns, as discussed above, a minor

portion of these two predecessor radicals could react directly with G and generate signals in the transient spectra because of the extremely reactive nature of these two radicals in oxidizing G (*11*–*13*, *33*–*37*).

The possible direct oxidation of G by $SO_4^{-\bullet}$ or $Cl^\bullet$ can also be manifested by the room temperature kinetics of the formation of $G^{+\bullet}/G(-H)^\bullet$ radicals. As shown in Fig. 2F, the growth of the transient absorbance at 510 nm associated with the $G^{+\bullet}/G(-H)^\bullet$ radicals is characterized by two kinetic components. The slow component is correlated with the 340-nm decay of $Cl_2^{-\bullet}$ (Fig. 2F) and, hence, corresponds to the oxidation of G by $Cl_2^{-\bullet}$. The rate constant derived from the slow component (~1×10^8 M^{-1} s^{-1}) is consistent with that reported for the $Cl_2^{-\bullet}$ + G reaction (*38*). In contrast, the fast component is beyond the time resolution of the experiment (nanoseconds) and supposedly ascribed to a faster oxidizing reaction, either $SO_4^{-\bullet}$ + G (Eq. 5) or $Cl^\bullet$ + G (Eq. 6). The reaction rate constant of $SO_4^{-\bullet}$ + G (Eq. 5) is 7.2×10^9 M^{-1} s^{-1} (*33*). The reaction rate constant of $Cl^\bullet$ with heteroaromatic compounds is two to three orders of magnitude larger than that found for $Cl_2^{-\bullet}$, falling into the diffusion-controlled limit (*35*–*37*).

Furthermore, the control experiment (fig. S1) points only to the $Cl^\bullet$ + G reaction as the source to the strong 570-nm transient and rules out the reaction of $SO_4^{-\bullet}$ + G as the contributor. This new 570-nm transient can be reasonably ascribed to a low stability intermediate of the $Cl^\bullet$ + G reaction, given the fact that $Cl^\bullet$ is known to have the tendency of forming adducts with aromatic compounds (benzene, pyridine, etc.), leading to a short-lived weakly bound π-complex or σ*-complex (*35*, *37*, *39*). For the reaction of $Cl^\bullet$ with pyridine, it was suggested that the Cl-pyridine complex may involve weak electron donation by the pyridine to $Cl^\bullet$ (*35*), similar to the charge separation predicted for the OH-guanine adduct that leads to the ion-pair intermediate $G^{+\bullet}\cdots OH^-$ (*22*). Analogously, G is a heteroaromatic compound and its reaction with $Cl^\bullet$ should proceed through addition mechanism and result into an adduct with the ion-pair ($G^{+\bullet}\cdots Cl^-$) character (Fig. 1).

Is the transient feature at 570 nm ascribed to the ion-pair intermediate $G^{+\bullet}\cdots Cl^-$? To aid the assignment, we performed CAM-B3LYP/6-311++G** level of calculations to characterize the structure and spectral properties of the ion-pair $G^{+\bullet}\cdots Cl^-$. According to the fully optimized geometry (Fig. 3A), $G^{+\bullet}\cdots Cl^-$ adopts a configuration in which the Cl atom is situated above the C4=C5 bond at a distance of 2.8 and 2.6 Å from C4 and C5 atoms of guanine. Vibrational frequencies for this complex are all positive, confirming its identity as a metastable intermediate but not as a transition state structure. Furthermore, the calculations of charge distribution and spin density (Fig. 3, A, C, and D) characterize the nature of this complex as the ion-pair $G^{+\bullet}\cdots Cl^-$. On the basis of the fully optimized geometry, the vertical excited-state ultraviolet-visible (UV-Vis) spectra for $G^{+\bullet}\cdots Cl^-$ were calculated, and two absorption bands predicted (Fig. 3B). The intense absorption band in the visible at 584 nm (47β→48β transition, ππ* in nature) has a much larger oscillator strength (f = 0.115) than the weak band in the UV at 329 nm (42β→48β transition, ππ*, f = 0.042) (Fig. 3B, fig. S2, and table S1). The predicted strong transition at 584 nm coincides with the intense 570-nm absorption band observed at low temperatures (Fig. 2D), corroborating the spectral assignment for the ion-pair transient $G^{+\bullet}\cdots Cl^-$. These results agree well with the TD-DFT calculations for the analogous species $G^{+\bullet}\cdots OH^-$ (with absorption maxima at ~580 nm) in the reaction of $OH^\bullet$ with G (*22*).

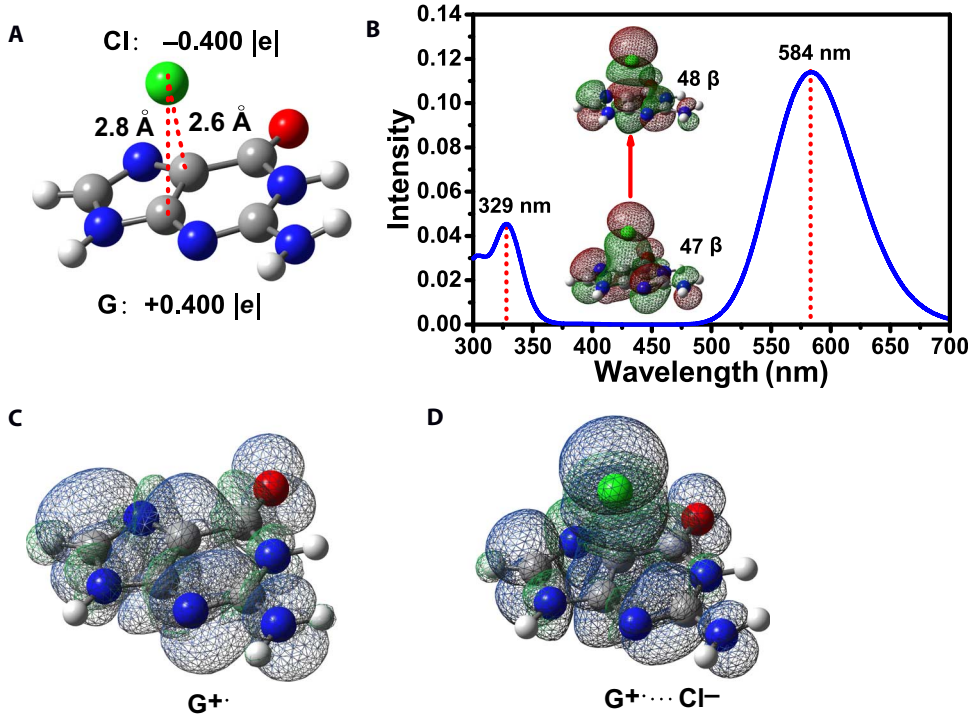

Fig. 3. Computation results. (**A**) Geometry of the ion-pair $G^{+\bullet}\cdots Cl^-$ optimized at the CAM-B3LYP/6-311++G** level. Charge distribution analyzed through the natural bond orbital (NBO) scheme at the same level is indicated. (**B**) TD-CAM-B3LYP/6-311++G** calculated absorption spectrum of $G^{+\bullet}\cdots Cl^-$. MOs corresponding to the transition at 584 nm are also shown. Spin density distributions of $G^{+\bullet}$ (**C**) and $G^{+\bullet}\cdots Cl^-$ (**D**). NBO and spin density analysis confirms the ion-pair $G^{+\bullet}\cdots Cl^-$ nature, showing that, upon the complex formation, charge separation occurs between G (+0.4|e|) and Cl (–0.4|e|), and the spin density is transferred from Cl to G, with the unpaired spin being largely localized on the guanine moiety as that for $G^{+\bullet}$. Carbon, oxygen, nitrogen, chlorine, and hydrogen atoms are denoted with gray, red, blue, green, and white balls, respectively.

Thus, the much stronger absorption in the visible (~580 nm) than in the UV is specific to the ion-pair species, whereas $G^{+\bullet}$ alone absorbs weakly at ~500 nm but strongly in the UV region (300 to 400 nm) (*33*, *34*).

It shows here for $G^{+\bullet}\cdots Cl^-$ and in previous theoretical work for $G^{+\bullet}\cdots OH^-$ that the ion-pair species result in a distinct absorption band in the visible region compared to $G^{+\bullet}$ alone (*22*). This can be understood from quantum theory in terms of Fermi's golden rule ($\lambda \propto |H|^2$). The transition probability λ is proportional to the square of the "matrix element" for the transition *H*, which represents the strength of the coupling between the initial and final state of a system. If the molecular orbitals (MOs), corresponding to the initial state and final state, overlap strongly in space, the transition would have large matrix elements, *H*. Therefore, an electronic transition will proceed more easily in view of this type of electron distribution. For free $G^{+\bullet}$, the main MOs involved in the transition at longer wavelengths overlap weakly (fig. S3). In contrast, the relevant MOs in the ion-pair $G^{+\bullet}\cdots Cl^-$ (fig. S2) and those in $G^{+\bullet}\cdots OH^-$ (*22*) overlap strongly in space due to the interaction of Cl or OH with C4=C5 of G and thus enable a characteristic strong transition in the visible wavelength region for this ion-pair species.

Presumably, the ion-pair species is organized and stabilized on the basis of the electrostatic attraction between cation and anion (*25*, *26*). The decay of the 570-nm band should then correspond to the ion-pair dissociation into the separated ions of $G^{+\bullet}$ and Cl^-, which is accompanied by the $G^{+\bullet}$ deprotonation, as evidenced by the transformation of the initial ion-pair absorption feature at 0.1 μs into the spectral pattern of G(-H)$^\bullet$ eventually at ~200 μs (Fig. 2D).

By capturing the ion-pair $G^{+\bullet}\cdots Cl^-$, the reaction mechanisms of $Cl^\bullet$ with G can be elucidated as an addition/charge separation process (Fig. 1), in which $Cl^\bullet$ is added to the C4=C5 double bond of G and charge separation results into $G^{+\bullet}\cdots Cl^-$, the crucial ion-pair intermediate toward the end products. This reaction route is quite similar to that of $OH^\bullet$ with G but is different from the direct one-electron oxidation reaction of $Cl_2^{-\bullet}$ or $SO_4^{-\bullet}$ with G (Eqs. 4 and 5) (*1*, *9*–*13*, *33*, *34*). It indicates that the oxidation damage reaction of G may follow the addition/charge separation mechanism for radicals ($Cl^\bullet$ and $OH^\bullet$) that are highly oxidizing and have a strong tendency of forming adducts with aromatic or heteroaromatic compounds. Thus, by capture of the $G^{+\bullet}\cdots Cl^-$ ion-pair intermediate, we provide direct evidence to establish the intricate addition/charge separation mechanism for the radical oxidation reaction of G, which is different from the direct one-electron oxidation mechanism normally adopted before.

Significantly, our experiments here identify that the spectral signature of the radical ion pair ($G^{+\bullet}\cdots Cl^-$) is different from that of $G^{+\bullet}$. The former is featured with a markedly intense absorption band at 570 nm, whereas the latter only absorbs weakly at 500 nm (*33*, *34*). Both species are important hole carrier intermediates invoked in DNA charge injection and charge transport (*40*) but were hardly discerned from each other before. In a recent study of the DNA charge transport in diphenylacetylenedicarboxamide (DPA)–A_nG hairpins induced by excitation of the integrated photosensitizer DPA (*40*), a band at 575 nm was observed in the femtosecond transient absorption spectra, and its difference from the spectral pattern of $G^{+\bullet}$ was also noticed but was still assigned to $G^{+\bullet}$ in terms of charge delocalization. In the experiment, the 575-nm band was only observed in DPA-G and DPA-A_1G, and none in other DPA-A_nG hairpins when the number of intervening adenine A increased to $n = 2$ to 6 which is an indication that the 575-nm band could be very likely ascribed to the contact ion pair of $DPA^{-\bullet}$–$G^{+\bullet}$ and $DPA^{-\bullet}$–$A_1G^{+\bullet}$. With the increasing number of intervening A, the electrostatic attraction between $DPA^{-\bullet}$ and $G^{+\bullet}$ is weakened such that the ion-pair spectral feature is removed. Our explicit characterization for the spectral signature of the radical ion pair here can be used to identify this type of important species and distinguish them from other possibly involved transients [$G^{+\bullet}$, G(-H)$^\bullet$, etc.] in guanine oxidation or DNA hole transfer.

Ion-pair spectra as exquisite markers for tracking the dynamics of intrabase-pair proton transfer in dsDNA oligonucleotides

We find further that the spectral signature for the ion-pair transient is highly sensitive to the interaction of base pairing in the DNA double helix, where each G base is paired with cytosine (C) through hydrogen bonding. Figure 4 displays the transient spectra measured for dsDNA $(GC)_6$ being oxidized by $Cl^\bullet/Cl_2^{-\bullet}$. The self-complementary sequence $(GC)_6$ was used here to ensure identical surroundings for each G or C base in the double helix. At room temperature (Fig. 4A), the spectra are essentially the same as those of the G base monomer oxidation (Fig. 2C). The decay of $Cl_2^{-\bullet}$ at 340 nm is accompanied by the buildup of the $G^{+\bullet}$/G(-H)$^\bullet$ radicals at 310, 390, and 510 nm, corresponding to the one-electron oxidation of G by $Cl_2^{-\bullet}$ in dsDNA. When probed at low temperatures, however, the spectra exhibit features different from those for the G base monomer. As seen in Fig. 4B, the characteristic peak at 570 nm for $G^{+\bullet}\cdots Cl^-$ splits into two intense bands peaking at 480 and 610 nm, respectively. The intensities of these two bands increase with the lowering of the temperature (Fig. 4C), consistent with the feature of an intermediate that can only be stabilized and captured at low temperatures, most likely the metastable ion pair involved in the radical oxidation of dsDNA $(GC)_6$.

First, the transient feature at 480 and 610 nm should only be correlated to the oxidation of the G base in the dsDNA $(GC)_6$. G in the GC pair should be oxidized in preference to C due to the much lower oxidation potential of G (~1.29 V) relative to C (~1.6 V). Moreover, calculations have revealed that GC has a much lower ionization potential value than the individual purine bases, with that of C being raised and G being lowered (*41*, *42*). Control experiments for the oxidation of pure C bases yielded no detectable signals in the transient spectra, neither at room temperature nor at low temperatures, indicating that the C bases in DNA sequence are not involved in the oxidation reaction associated with ion-pair formation. Even assuming that addition occurs with $Cl^\bullet$ + C, no charge separation is expected to occur as it did for guanine because of the much higher oxidation potential of cytosine.

Second, if it is ascribed to the ion-pair transient, why does the single absorption peak for $G^{+\bullet}\cdots Cl^-$ at 570 nm with G base monomer split into two bands at 480 and 610 nm in the case of the dsDNA $(GC)_6$? A control experiment was performed for the oligonucleotide-$(GCGT)_3$, which can only form single-stranded DNA (ssDNA). The transient spectra obtained for the reaction of ssDNA + $Cl^\bullet/Cl_2^{-\bullet}$ at 230 K capture only a single absorption band around 570 nm (fig. S4), which is similar to the case for the G base monomer. The absence of the spectral splitting for the ion pair in ssDNA suggests that the base-pairing effect should be responsible for the two bands at 480 and 610 nm with the dsDNA $(GC)_6$. In dsDNA when $G^{+\bullet}$ is formed, the effect of base pairing is to transfer the N1 proton of $G^{+\bullet}$ to N3 of C (the so-called intrabase-pair proton transfer; Fig. 5A) because the protonation pK_a of N3 in C (4.3) is slightly higher than

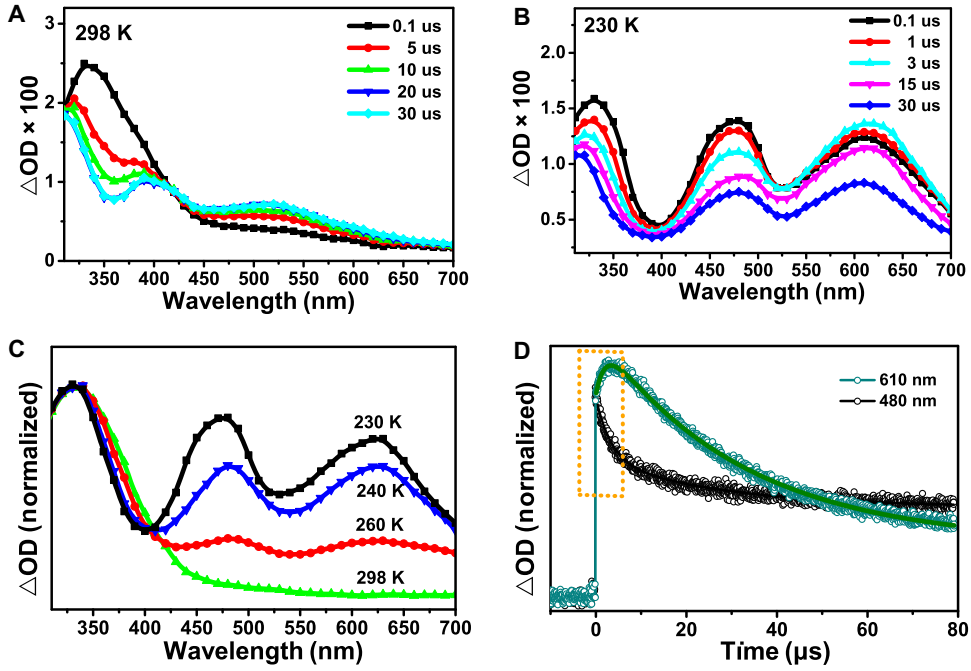

Fig. 4. Oxidation of G in dsDNA. Transient absorption spectra obtained at 298 K (**A**) and at 230 K (**B**) after 355-nm laser flash photolysis of $Na_2S_2O_8$ + LiCl + dsDNA. (**C**) Time slice (0.1 μs) of the transient absorption spectra obtained after 355-nm laser flash photolysis of $Na_2S_2O_8$ + LiCl + dsDNA at different temperatures. (**D**) Kinetic curves monitored at 480 and 610 nm after laser flash photolysis of $Na_2S_2O_8$ + LiCl + dsDNA at 230 K, with the biexponential fits to the data (solid lines). The concentration of $Na_2S_2O_8$, LiCl, and dsDNA used in above experiments is 150 mM, 7.0 M, and 0.1 mM, respectively.

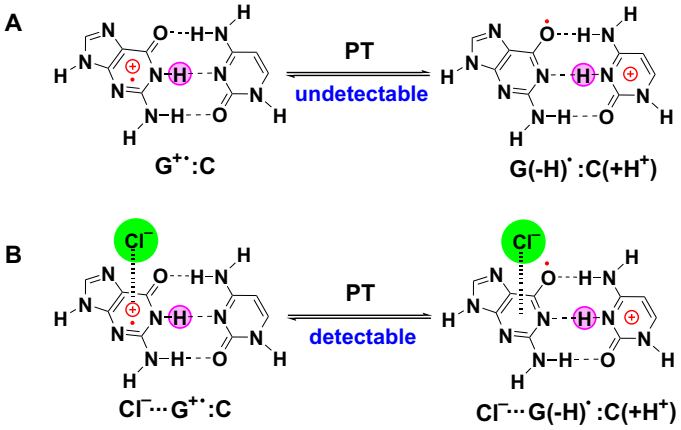

Fig. 5. PT mechanism. Schematic diagram of the proton transfer (PT) along the central hydrogen bond from $G^{+\bullet}$ to C within G:C base pair (**A**) and when a nearby Cl^- is attached (**B**).

that of N1 in $G^{+\bullet}$ (3.9) (*1*). A prototropic equilibrium (K_{eq}, ~2.5 at room temperature) exists within the $G^{+\bullet}$:C base pair, where $G^{+\bullet}$ only partially transfers its N1 proton (H^+) to the N3 site on cytosine (C), forming the proton-transferred species G(-H)•:C(+H^+) (Fig. 5A) (*1*, *6*, *9*, *11*, *12*, *33*, *34*). Therefore, the two protonated structures $G^{+\bullet}$:C and G(-H)•:C(+H^+) in equilibrium possibly lead to two different ion-pair species when the Cl^- is attached nearby. Given that the characteristic transition in the visible wavelength for the ion-pair species $G^{+\bullet}\cdots Cl^-$ results from the strong electrostatic interaction on MOs, the absorption peak wavelength should be different for the two ion-pair species $Cl^-\cdots G^{+\bullet}$:C↔$Cl^-\cdots$G(-H)•:C(+H^+) when the positive charge is shifted from G to C after the intrabase-pair proton transfer (Fig. 5B). As a result, two strong absorption peaks (480 and 610 nm) for these two forms of ion pair are observed in dsDNA $(GC)_6$. The peak shift of these two ion-pair forms in dsDNA relative to free $G^{+\bullet}\cdots Cl^-$ in G base monomer should also be related to π-stacking interactions of the neighboring bases along the strand.

Meanwhile, it shows in the first few microseconds (~3 μs) of the transient spectra (Fig. 4, B and D) that the decay of the 480-nm band is concomitant with the growth of the 610-nm band. This gives a hint that the process may correspond to the intrabase-pair proton transfer with the transformation from $Cl^-\cdots G^{+\bullet}$:C (480 nm) to $Cl^-\cdots$G(-H)•:C(+H^+) (610 nm). After ~3 μs, the prototropic equilibria are reached, and the two ion-pair species decay monotonically at the time scale of tens of microseconds, which should correspond to the ion-pair dissociation to separated ions of Cl^- and $G^{+\bullet}$:C or G(-H)•:C(+H^+). The decay of the ion pair in dsDNA is faster than that in the G base monomer, probably because the negative PO_4^{3-} groups in the DNA backbone tend to weaken the electrostatic attraction within the ion-pair species.

These postulated spectral assignments can be further supported by kinetic measurements. The kinetic curves of the 480- and 610-nm bands at 230 K are displayed in Fig. 4D. As shown, the transients at 480 nm involve a fast decay process and a slow one, which can be fitted by a biexponential function with rate constants of 3.9×10^5 and 3.0×10^4 s^{-1}, respectively. The larger rate constant (3.9×10^5 s^{-1}) is consistent with the rate (3.8×10^5 s^{-1}) obtained from the fast increase of 610 nm. These two rates as a function of temperature were measured. The Arrhenius plots yield an energy barrier in the range of 1.4 to 1.7 kcal/mol (Fig. 6, A and B), which agrees with the intrabase-pair proton transfer energy barrier calculated by DFT calculation (1.42 kcal/mol) (*43*). These results further confirm that the fast component is correlated to the proton transfer within the base pair $G^{+\bullet}$:C. In addition, the assignment of the 480-nm band to $Cl^-\cdots G^{+\bullet}$:C

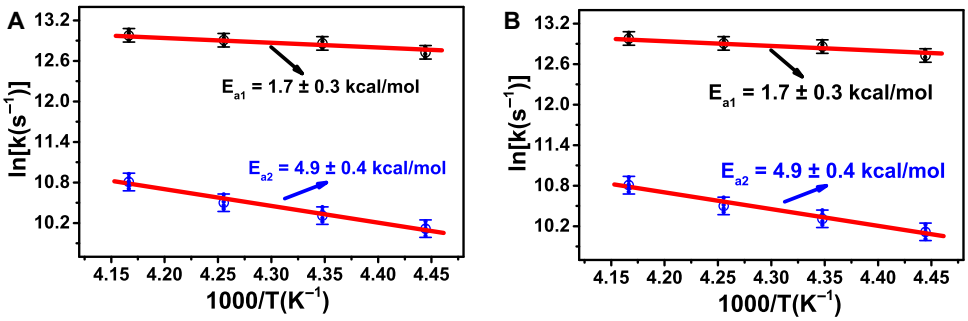

Fig. 6. Activation energy. Arrhenius plots for the temperature dependence (240, 235, 230, and 225 K) of the rate constants (black circle dots, fast phase; blue circle dots, slow phase) obtained from the absorbance changes at 480 nm (**A**) and 610 nm (**B**), with the activation energy indicated. Solid red line is the fit.

and the 610-nm band to $Cl^-\cdots G(-H)^\bullet{:}C(+H^+)$ is corroborated. Meanwhile, the slower phase of the 480- and 610-nm band should correspond to the ion-pair dissociation, and thus, the slope of the Arrhenius plots (4.7 to 4.9 kcal/mol) gives the dissociation energy of the ion pair (Fig. 6, A and B).

When $G^{+\bullet}$ is formed in dsDNA, the proton movement along the hydrogen bond within the GC base pair involves only a slight displacement of the equilibrium position of the bridging proton and thus, in principle, occurs very rapidly at room temperature (estimated reaction period, ≤1 ps) (*1*, *44*). It maintains the proton-shifted resonance structure $[G^{+\bullet}{:}C\leftrightarrow G(-H)^\bullet{:}C(+H^+)]$ until the proton of $C(+H^+)$ is released to the surrounding water (Fig. 5A) (*1*, *6*, *9*, *11*, *12*, *33*, *34*). In the pioneering work of Steenken, the pK_a of $G^{+\bullet}$ was estimated to be 3.9, and on the basis of the acidity of $G^{+\bullet}$ and basicity of C, a facile proton transfer reaction from N1 of guanine to hydrogen-bonded cytosine within the GC base pair was proposed (*1*, *9*). Later on, nanosecond pulse radiolysis experiments were performed to examine the proton transfer reactions in one electron-oxidized dsDNA oligonucleotides (*33*, *34*). By following the weak absorbance change at 625 nm due to deprotonation of $G^{+\bullet}$ to $G(-H)^\bullet$, the overall proton transfer process from $G^{+\bullet}$ to C within GC base pair and from $C(+H^+)$ to the surrounding water was monitored (*33*, *34*). The measured deprotonation rate constants on the order of 10^6 to 10^7 s^{-1} reflect largely the second step of proton release to water, which is the rate-limiting one, whereas the first step of intrabase-pair proton transfer takes place on an approximately picosecond time scale (*1*, *44*) and could not be directly probed by pulse radiolysis. More recently, serial studies with ESR at low temperatures characterized various protonation forms of the one-electron oxidized GC pair in dsDNA (*11*). By selective deuteration at C-8 on guanine moiety, ESR spectra at low temperatures identified that the one-electron oxidized G in dsDNA exists as $G(N1–H)^\bullet$ or, more accurately, $G(N1–H)^\bullet{:}C(+H^+)$, providing evidence for the occurrence of the intrabase-pair proton transfer. In agreement with the experiment, DFT calculations in the presence of 6 or 11 explicit waters have shown that the free energy for intrabase-pair proton transfer in $G^{+\bullet}{:}C$ becomes favorable upon inclusion of water (ΔG = –0.65 kcal/mol) (*43*). The zero-point energy–corrected energy barrier for this process was calculated to be 1.42 kcal/mol.

As discussed above, although extensively examined, there is yet no direct experimental detection for the intrabase-pair proton transfer process in real time, owing to the extremely fast rate (estimated reaction period, ≤1 ps) and the fact that the two protonated forms in the chemical equilibrium cannot be distinguished easily with similar spectra (Fig. 5A). Here, we have observed the metastable ion-pair intermediates $Cl^-\cdots G^{+\bullet}{:}C\leftrightarrow Cl^-\cdots G(-H)^\bullet{:}C(+H^+)$ involved in oxidized dsDNA by means of laser flash photolysis measurements at low temperatures. The sensitive electrostatic interactions of the nearby Cl^- on MOs make the two protonated forms in GC pair distinguishable, with two intense absorption peaks (480 and 610 nm) being resolved in the time-resolved spectra. In addition, slowing down the reaction rate at low temperatures, enables the detection of the intrabase-pair proton transfer process (Fig. 4, B and D). In addition to providing direct spectral evidence, the real-time monitoring allows, for the first time, the kinetic determination of the energy barrier for this process (1.4 to 1.7 kcal/mol). The measured energy barrier agrees well with the high-level computational predictions (1.42 kcal/mol) (*43*). Such a low barrier further demonstrates the facile occurrence of intrabase-pair proton transfer (approximately in picoseconds) and its coupling to hole or electron transfer (10^8 to 10^{12} s^{-1}). The mechanisms of long-range charge transfer in DNA moderated by proton transfer (*5*, *11*, *43*) can thus be substantiated further. Overall, it shows here that the unique spectral feature of an ion pair, which has intense absorption at visible wavelengths and is sensitive to the protonation equilibria, acts as an exquisite probe to characterize the intrabase-pair proton transfer dynamics in dsDNA.

CONCLUSION

In summary, by combining the techniques of cryogenic stabilization and time-resolved laser flash photolysis spectroscopy, we have successfully captured the radical ion-pair transient $G^{+\bullet}\cdots Cl^-$ in the oxidation of guanine in free deoxynucleoside and in dsDNA oligonucleotides by chlorine radicals, providing direct evidence to establish the intricate addition/charge separation mechanism underlying DNA guanine oxidation that is distinct from the direct one-electron oxidation mechanism adopted before. In particular, the unique spectral signature associated with the radical ion-pair $G^{+\bullet}\cdots Cl^-$ is identified, revealing a markedly intense absorption feature peaking at 570 nm in the transient spectra. The strong visible and weak UV absorption pattern is found to be specific to the ion-pair species, providing key knowledge to distinguish the ion pair from other possibly involved transient radicals [$G^{+\bullet}$, $G(-H)^\bullet$, etc.] in guanine oxidation or DNA hole transfer. Significantly, examination with the oxidized dsDNA $(GC)_6$ reveals that the ion-pair spectrum is highly sensitive to the protonation equilibria within the $G^{+\bullet}{:}C$ base pair, splitting into two resolved bands at 480 and 610 nm that correspond to the two protonated forms in equilibrium $Cl^-\cdots G^{+\bullet}{:}C\leftrightarrow Cl^-\cdots G(-H)^\bullet{:}C(+H^+)$. By placement of a nearby counterion Cl^-, the two protonated forms are allowed to be discerned spectroscopically. The unique ion-pair spectral signature thus provides exquisite

markers for tracking the dynamics of intrabase-pair proton transfer in dsDNA that is a critical factor in moderating long-range hole transfer in DNA. By capture of the radical ion pair and explicit identification of its spectroscopic signature, the present work provides direct evidence to ascertain the formation of this crucial intermediate in DNA guanine oxidation and paves the way to study intricate molecular mechanisms in DNA damage and DNA charge transfer using the ion-pair spectroscopic signature.

MATERIALS AND METHODS

Materials

dG (Alfa Aesar), sodium persulfate ($Na_2S_2O_8$; Sigma-Aldrich), sodium perchlorate ($NaClO_4$; Sigma-Aldrich), 2′-deoxycytidine (Sigma), and lithium chloride (LiCl; Aladdin) were used as purchased without further purification. The DNA oligonucleotides $(GC)_6$ and $(GTGC)_3$ were purchased from Sangon Biotech (Shanghai) Co. Ltd. in the polyacrylamide gel electrophoresis–purified form. Single-strand concentrations were determined by monitoring the absorbance at 260 nm in the UV-Vis spectra and using the corresponding extinction coefficients of 101,100 and 107,400 M^{-1} cm^{-1} for $(GC)_6$ and $(GTGC)_3$, respectively. The sample of dG or the DNA oligonucleotide was dissolved in solution of LiCl (7.0 M) in H_2O. The dsDNA oligomers in homogeneous aqueous glasses (7.5 M LiCl) have been reported to be in the B conformation (*12*). Thus, in our system (homogeneous solutions of oligomers in 7.0 M LiCl), the self-complementary oligomers $(GC)_6$ formed a dsDNA conformation. Ultrapure water obtained by Millipore filtration was used as solvent. A total of ~120 or 20 mg of $Na_2S_2O_8$ was added as the precursor of the initial oxidation radical, which triggered subsequent reactions.

Laser flash photolysis

Nanosecond time-resolved transient absorption spectra were measured using a flash photolysis setup Edinburgh LP920 spectrometer (Edinburgh Instruments Ltd.) combined with a Nd:YAG laser (Spectra-Physics Lab 170, Newport Corp.). Each measurement was performed in a 1-cm-pathlength quartz cuvette that was put in the Oxford Instruments OptistatDN cryostat and cooled to a certain temperature. The sample was excited by a 355-nm laser pulse (1 Hz; 10 mJ per pulse; full width at half maximum, ≈7 ns). The analyzing light was from a 450-W pulsed xenon lamp. A monochromator equipped with a photomultiplier for collecting the spectral range from 300 to 700 nm was used to analyze the transient absorption spectra. The signals from the photomultiplier were displayed and recorded as a function of time on a 100-MHz (1.25 Gs/s sampling rate) oscilloscope (TDS 3012C, Tektronix), and the data were transferred to a PC. Data were analyzed with online software of the LP920 spectrophotometer. The fitting quality was judged by weighted residuals and reduced χ^2 value.

The concentration of radicals generated by a single laser pulse (~6.8 μM), estimated by the $SO_4^{-\bullet}$ absorbance at 450 nm using an extinction coefficient of 1600 M^{-1} cm^{-1}, was much lower than that of G in free deoxynucleoside (4 mM) or oligonucleotides (1.2 mM), excluding the occurrence of sequential oxidation events of guanine.

Calculation methods

The geometry was fully optimized at the CAM-B3LYP/6-311++G** level of theory. The vertical excited-state UV-Vis spectrum of the ion pair was calculated using the TD CAM-B3LYP method based on the geometry optimized at the same level. We used the TD CAM-B3LYP method for geometry optimization and excited-state calculations because the B3LYP functional is not appropriate for long-range interaction involving charge transfer excited states (*22*, *45*). The transition energies for charge transfer states are greatly underestimated by the B3LYP method especially as the distance increases (*22*, *45*, *46*). The CAM-B3lYP method is a long-range corrected hybrid functional and found to be very successful for studying the excited state of systems involving charge transfer states (*46*). All the calculations were carried out using the Gaussian 09 program package (*47*). GaussView molecular modeling software was used to plot the MOs and draw the molecular structure.

SUPPLEMENTARY MATERIALS

Supplementary material for this article is available at http://advances.sciencemag.org/cgi/content/full/3/6/e1700171/DC1

fig. S1. Oxidation of G by $SO_4^{-\bullet}$.

fig. S2. MOs mainly involved in the electronic transitions of $G^{+\bullet}\cdots Cl^-$ computed at the TD-CAM-B3LYP/6-311++G**//CAM-B3LYP/6-311++G** level.

fig. S3. MOs mainly involved in the electronic transitions of $G^{+\bullet}$ computed at the TD-CAM-B3LYP/6-311++G**//CAM-B3LYP/6-311++G** level.

fig. S4. Oxidation of G in ssDNA.

table S1. Vertical optical transitions of $G^{+\bullet}\cdots Cl^-$ and $G^{+\bullet}$ computed at the TD-CAM-B3LYP/6-311++G**//CAM-B3LYP/6-311++G** level.

REFERENCES AND NOTES

1. S. Steenken, Purine bases, nucleosides, and nucleotides: Aqueous solution redox chemistry and transformation reactions of their radical cations and e^- and OH adducts. *Chem. Rev.* **89**, 503–520 (1989).
2. J. Cadet, T. Douki, J.-L. Ravanat, Oxidatively generated damage to the guanine moiety of DNA: Mechanistic aspects and formation in cells. *Acc. Chem. Res.* **41**, 1075–1083 (2008).
3. E. Meggers, M. E. Michel-Beyerle, B. Giese, Sequence dependent long range hole transport in DNA. *J. Am. Chem. Soc.* **120**, 12950–12955 (1998).
4. J. J. Storhoff, C. A. Mirkin, Programmed materials synthesis with DNA. *Chem. Rev.* **99**, 1849–1862 (1999).
5. Y. Osakada, K. Kawai, M. Fujitsuka, T. Majima, Charge transfer through DNA nanoscaled assembly programmable with DNA building blocks. *Proc. Natl. Acad. Sci. U.S.A.* **103**, 18072–18076 (2006).
6. L. P. Candeias, S. Steenken, Ionization of purine nucleosides and nucleotides and their components by 193-nm laser photolysis in aqueous solution: Model studies for oxidative damage of DNA. *J. Am. Chem. Soc.* **114**, 699–704 (1992).
7. M. K. Kuimova, A. J. Cowan, P. Matousek, A. W. Parker, X. Z. Sun, M. Towrie, M. W. George, Monitoring the direct and indirect damage of DNA bases and polynucleotides by using time-resolved infrared spectroscopy. *Proc. Natl. Acad. Sci. U.S.A.* **103**, 2150–2153 (2006).
8. A. B. Stephansen, S. B. King, Y. Yokoi, Y. Minoshima, W.-L. Li, A. Kunin, T. Takayanagi, D. M. Neumark, Dynamics of dipole-and valence bound anions in iodide-adenine binary complexes: A time-resolved photoelectron imaging and quantum mechanical investigation. *J. Chem. Phys.* **143**, 104308 (2015).
9. L. P. Candeias, S. Steenken, Structure and acid-base properties of one-electron-oxidized deoxyguanosine, guanosine, and 1-methylguanosine. *J. Am. Chem. Soc.* **111**, 1094–1099 (1989).
10. J. Cadet, T. Douki, J.-L. Ravanat, One-electron oxidation of DNA and inflammation processes. *Nat. Chem. Biol.* **2**, 348–349 (2006).
11. A. Adhikary, D. Khanduri, M. D. Sevilla, Direct observation of the hole protonation state and hole localization site in DNA-oligomers. *J. Am. Chem. Soc.* **131**, 8614–8619 (2009).
12. A. Adhikary, A. Kumar, S. A. Munafo, D. Khanduri, M. D. Sevilla, Prototropic equilibria in DNA containing one-electron oxidized GC: Intra-duplex vs. Duplex to solvent deprotonation. *Phys. Chem. Chem. Phys.* **12**, 5353–5368 (2010).
13. Y. Rokhlenko, N. E. Geacintov, V. Shafirovich, Lifetimes and reaction pathways of guanine radical cations and neutral guanine radicals in an oligonucleotide in aqueous solutions. *J. Am. Chem. Soc.* **134**, 4955–4962 (2012).
14. N. C. Seeman, Nucleic acid nanostructures and topology. *Angew. Chem. Int. Ed.* **37**, 3220–3238 (1998).
15. T. Lindahl, Instability and decay of the primary structure of DNA. *Nature* **362**, 709–715 (1993).

16. L. I. Shukla, A. Adhikary, R. Pazdro, D. Becker, M. D. Sevilla, Formation of 8-oxo-7,8-dihydroguanine-radicals in γ-irradiated DNA by multiple one-electron oxidations. *Nucleic Acids Res.* **32**, 6565–6574 (2004).
17. J. P. Hall, F. E. Poynton, P. M. Keane, S. P. Gurung, J. A. Brazier, D. J. Cardin, G. Winter, T. Gunnlaugsson, I. V. Sazanovich, M. Towrie, C. J. Cardin, J. M. Kelly, S. J. Quinn, Monitoring one-electron photo-oxidation of guanine in DNA crystals using ultrafast infrared spectroscopy. *Nat. Chem.* **7**, 961–967 (2015).
18. P. Changenet-Barret, T. Gustavsson, D. Markovitsi, I. Manet, Ultrafast electron transfer in complexes of doxorubicin with human telomeric G-quadruplexes and GC duplexes probed by femtosecond fluorescence spectroscopy. *Chemphyschem* **17**, 1264–1272 (2016).
19. S. Fröbel, L. Levi, S. M. Ulamec, P. Gilch, Photoinduced electron transfer between psoralens and DNA: Influence of DNA sequence and substitution. *Chemphyschem* **17**, 1377–1386 (2016).
20. P. M. Keane, F. E. Poynton, J. P. Hall, I. V. Sazanovich, M. Towrie, T. Gunnlaugsson, S. J. Quinn, C. J. Cardin, J. M. Kelly, Reversal of a single base-pair step controls guanine photo-oxidation by an intercalating ruthenium(II) dipyridophenazine complex. *Angew. Chem. Int. Ed.* **54**, 8364–8368 (2015).
21. S. Fröbel, A. Reiffers, C. Torres Ziegenbein, P. Gilch, DNA intercalated psoralen undergoes efficient photoinduced electron transfer. *J. Phys. Chem. Lett.* **6**, 1260–1264 (2015).
22. A. Kumar, V. Pottiboyina, M. D. Sevilla, Hydroxyl radical ($OH^•$) reaction with guanine in an aqueous environment: A DFT study. *J. Phys. Chem. B* **115**, 15129–15137 (2011).
23. L. P. Candeias, S. Steenken, Reaction of $HO^•$ with guanine derivatives in aqueous solution: Formation of two different redox-active OH-adduct radicals and their unimolecular transformation reactions. Properties of $G(-H)^•$. *Chem. Eur. J.* **6**, 475–484 (2000).
24. W.-M. Kwok, C. Ma, D. L. Phillips, Femtosecond time- and wavelength-resolved fluorescence and absorption spectroscopic study of the excited states of adenosine and an adenine oligomer. *J. Am. Chem. Soc.* **128**, 11894–11905 (2006).
25. M. Szwarc, Ions and ion pairs. *Acc. Chem. Res.* **2**, 87–96 (1969).
26. Y. Marcus, G. Hefter, Ion pairing. *Chem. Rev.* **106**, 4585–4621 (2006).
27. Y. Wu, C. J. Mundy, M. E. Colvin, R. Car, On the mechanisms of OH radical induced DNA-base damage: A comparative quantum chemical and Car–Parrinello molecular dynamics study. *J. Phys. Chem. A* **108**, 2922–2929 (2004).
28. A. W. Parker, C. Y. Lin, M. W. George, M. Towrie, M. K. Kuimova, Infrared characterization of the guanine radical cation: Finger printing DNA damage. *J. Phys. Chem. B* **114**, 3660–3667 (2010).
29. L. Wu, K. Liu, J. Jie, D. Song, H. Su, Direct observation of guanine radical cation deprotonation in G-quadruplex DNA. *J. Am. Chem. Soc.* **137**, 259–266 (2015).
30. W. J. McElroy, A laser photolysis study of the reaction of SO_4^- with Cl^- and the subsequent decay of Cl_2^- in aqueous solution. *J. Phys. Chem.* **94**, 2435–2441 (1990).
31. V. Nagarajan, R. W. Fessenden, Flash photolysis of transient radicals. 1. X_2^- with X = Cl, Br, I, and SCN. *J. Phys. Chem.* **89**, 2330–2335 (1985).
32. G. G. Jayson, B. J. Parsons, A. J. Swallow, Some simple, highly reactive, inorganic chlorine derivatives in aqueous solution. Their formation using pulses of radiation and their role in the mechanism of the Fricke dosimeter. *J. Chem. Soc. Faraday Trans.* **69**, 1597–1607 (1973).
33. K. Kobayashi, S. Tagawa, Direct observation of guanine radical cation deprotonation in duplex DNA using pulse radiolysis. *J. Am. Chem. Soc.* **125**, 10213–10218 (2003).
34. K. Kobayashi, R. Yamagami, S. Tagawa, Effect of base sequence and deprotonation of guanine cation radical in DNA. *J. Phys. Chem. B* **112**, 10752–10757 (2008).
35. R. Breslow, M. Brandl, J. Hunger, N. Turro, K. Cassidy, K. Krogh-Jespersen, J. D. Westbrook, Pyridine complexes of chlorine atoms. *J. Am. Chem. Soc.* **109**, 7204–7206 (1987).
36. Z. B. Alfassi, S. Mosseri, P. Neta, Reactivities of chlorine atoms and peroxyl radicals formed in the radiolysis of dichloromethane. *J. Phys. Chem.* **93**, 1380–1385 (1989).
37. B. Praña, R. Gomperts, J. A. Sordo, A theoretical study on the mechanism of the reaction between Cl atoms and nitrobenzene. *Chem. Phys. Lett.* **392**, 236–241 (2004).
38. J. F. Ward, I. Kuo, Steady state and pulse radiolysis of aqueous chloride solutions of nucleic acid components. *Adv. Chem.* **81**, 368–373 (1968).
39. R. K. Khanna, B. Armstrong, H. Cui, J. M. Tanko, Inverted regioselectivities in the reactions of chlorine atoms with heteroarylmethanes. *J. Am. Chem. Soc.* **114**, 6003–6006 (1992).
40. M. A. Harris, A. K. Mishra, R. M. Young, K. E. Brown, M. R. Wasielewski, F. D. Lewis, Direct observation of the hole carriers in DNA photoinduced charge transport. *J. Am. Chem. Soc.* **138**, 5491–5494 (2016).
41. M. Hutter, T. Clark, On the enhanced stability of the guanine–cytosine base-pair radical cation. *J. Am. Chem. Soc.* **118**, 7574–7577 (1996).
42. X. Li, Z. Cai, M. D. Sevilla, Investigation of proton transfer within DNA base pair anion and cation radicals by density functional theory (DFT). *J. Phys. Chem. B* **105**, 10115–10123 (2001).
43. A. Kumar, M. D. Sevilla, Influence of hydration on proton transfer in the guanine–cytosine radical cation ($G^{•+}$–C) base pair: A density functional theory study. *J. Phys. Chem. B* **113**, 11359–11361 (2009).
44. A. Douhal, S. K. Kim, A. H. Zewail, Femtosecond molecular dynamics of tautomerization in model base pairs. *Nature* **378**, 260–263 (1995).
45. A. Dreuw, M. Head-Gordon, Single-reference ab initio methods for the calculation of excited states of large molecules. *Chem. Rev.* **105**, 4009–4037 (2005).
46. M. J. G. Peach, C. R. L. Sueur, K. Ruud, M. Guillaume, D. J. Tozer, TDDFT diagnostic testing and functional assessment for triazene chromophores. *Phys. Chem. Chem. Phys.* **11**, 4465–4470 (2009).
47. M. J. Frisch, G. W. Trucks, H. B. Schlegel, G. E. Scuseria, M. A. Robb, J. R. Cheeseman, G. Scalmani, V. Barone, B. Mennucci, G. A. Petersson, H. Nakatsuji, M. Caricato, X. Li, H. P. Hratchian, A. F. Izmaylov, J. Bloino, G. Zheng, J. L. Sonnenberg, M. Hada, M. Ehara, K. Toyota, R. Fukuda, J. Hasegawa, M. Ishida, T. Nakajima, Y. Honda, O. Kitao, H. Nakai, T. Vreven, J. A. Montgomery Jr., J. E. Peralta, F. Ogliaro, M. Bearpark, J. J. Heyd, E. Brothers, K. N. Kudin, V. N. Staroverov, T. Keith, R. Kobayashi, J. Normand, K. Raghavachari, A. Rendell, J. C. Burant, S. S. Iyengar, J. Tomasi, M. Cossi, N. Rega, J. M. Millam, M. Klene, J. E. Knox, J. B. Cross, V. Bakken, C. Adamo, J. Jaramillo, R. Gomperts, R. E. Stratmann, O. Yazyev, A. J. Austin, R. Cammi, C. Pomelli, J. W. Ochterski, R. L. Martin, K. Morokuma, V. G. Zakrzewski, G. A. Voth, P. Salvador, J. J. Dannenberg, S. Dapprich, A. D. Daniels, O. Farkas, J. B. Foresman, J. V. Ortiz, J. Cioslowski, D. J. Fox, *Gaussian 09, Revision B.01* (Gaussian Inc., 2009).

Acknowledgments

Funding: This work was financially supported by the National Natural Science Foundation of China (grant nos. 21425313, 21333012, and 91441108), the National Basic Research Program of China (2013CB834602), and the Chinese Academy of Sciences (project XDB12020200).
Author contributions: H.S. conceived the project and designed the experiments. J.J. designed and performed the experiments and implemented the computation. J.J., K.L., L.W., H.Z., D.S., and H.S. discussed the results and analyzed the data. H.S. supervised the study. H.S. and J.J. wrote the manuscript. **Competing interests:** The authors declare that they have no competing interests. **Data and material availability:** All data needed to evaluate the conclusions in the paper are present in the paper and/or the Supplementary Materials. Additional data related to this paper may be requested from the authors.

Submitted 17 January 2017
Accepted 6 April 2017
Published 2 June 2017
10.1126/sciadv.1700171

Citation: J. Jie, K. Liu, L. Wu, H. Zhao, D. Song, H. Su, Capturing the radical ion-pair intermediate in DNA guanine oxidation. *Sci. Adv.* **3**, e1700171 (2017).

Science Advances

Capturing the radical ion-pair intermediate in DNA guanine oxidation

Jialong Jie, Kunhui Liu, Lidan Wu, Hongmei Zhao, Di Song and Hongmei Su

Sci Adv **3** (6), e1700171.
DOI: 10.1126/sciadv.1700171